Preprints (www.preprints.org) | NOT PEER-REVIEWED | Posted: 20 January 2017 doi:10.20944/preprints201701.0091.v1

Peer-reviewed version available at Sensors 2017, 17, 535; doi:10.3390/s17030535

Article

Shock Pulse Index and Its Application in the Fault Diagnosis of Rolling Element Bearings

Peng Sun [1], Yuhe Liao [1,*] and Jin Lin [2]

[1] Shaanxi Key Laboratory of Mechanical Product Quality Assurance and Diagnostics, Xi'an Jiaotong University, Xi'an 710049, China; tracysun@stu.xjtu.edu.cn

[2] State Key Laboratory for Manufacturing Systems Engineering, Xi'an Jiaotong University, Xi'an 710049, China; jinglin@mail.xjtu.edu.cn

* Correspondence: yhliao@mail.xjtu.edu.cn; Tel.: +86-29-8266-7938

Abstract: Properties of time domain parameters of the vibration signal have been extensively studied for the fault diagnosis of rolling element bearings (REB). Parameters like kurtosis and Envelope Harmonic-to-Noise Ratio are most widely applied in this field and some important progress has been made. However, since only one-sided information is contained in these parameters respectively, problems still exist in practice when the signals collected are of complicated structure and/or contaminated by strong background noises. A new parameter, named Shock pulse index (SPI), is proposed in this paper. It integrates the mutual advantage of both parameters above and can help effectively identify fault related impulse components under the interference of strong background noises, unrelated harmonic components and random impulses. The SPI optimizes the parameters of Maximum Correlated Kurtosis Deconvolution (MCKD), which is used to filter the signals under consideration. Finally, the interested transient information contained in the filtered signal can be highlighted through demodulation with Teager Energy Operator (TEO). Fault related impulse components can therefore be extracted accurately. Simulations and experiment analyses verify the effectiveness and correctness of the SPI.

Keywords: fault diagnosis; shock pulse index; maximum correlated kurtosis deconvolution; teager energy operator; rolling element bearings.

1. Introduction

Rolling element bearings (REB) are widely used and the running health condition of the REB is of great importance to the operating stability and safety of the related machinery [1]. Therefore, study on the theory and method of the REB fault diagnosis has always been a hotspot in this research area. Many scholars and engineers around the world have made enormous efforts on this topic and great achievements have been obtained [2]. Different kinds of information, including vibration, acoustic, temperature and wear debris, are explored and investigated in the existing method to analyze the REB operating condition. Among all these researches, vibration analysis, as well as acoustic analysis, are most frequently used [3].

As to some of the vibration analysis based the REB fault diagnosis methods, how to effectively extract the fault feature related impulse components from the vibration signal is always the critical issue that needs to be solved first of all. Here the difficulty lies primarily in that, besides the fault feature frequency components, the vibration signal collected also contains some other interference components [4]. In some serious situations, especially at the early stage of the REB faults, useful information with comparatively low amplitude could even be totally submerged by strong background noises. Results of countless researches have proved the effectiveness of using signal characteristic parameters to distinguish interested fault related information from noise corrupted signal. Significant progress has been made in related research [5-7].

Considering the sensitivity to impact signal, which is the main characteristic of the faulty REB vibration, one of the time domain higher-order statistics, the kurtosis, is introduced here. It was first

Preprints (www.preprints.org) | NOT PEER-REVIEWED | Posted: 20 January 2017 doi:10.20944/preprints201701.0091.v1

Peer-reviewed version available at Sensors 2017, 17, 535; doi:10.3390/s17030535

studied by Dyer et al. and they suggested that it could indicate the emergence of bearing fault when the value of kurtosis is greater than 3 [8]. However, since they calculate the kurtosis directly with the noised vibration signal, the result could be interfered by the background noise. In view of this, Dwyer then proposed the Spectral kurtosis (SK), which can locate the impulse components in frequency domain, to solve this problem [9]. Based on that, Antoni [10-12] further studied the theory of the SK and put forward the Fast kurtogram for optimal resonance frequency band. Lei [13]introduced wavelet packet transform (WPT), which was used as a filter to replace the FIR filters, into kurtogram and the analysis accuracy was therefore improved. However, interference of strong non-Gaussian noise could still bring trouble to the SK technique and lead to incorrect results [2, 14]. Barszcz [14]then put forward a method named Protrugram which is capable of detecting transients with much smaller signal-to-noise ratio than that of the SK-based Fast kurtogram. The drawback of this method is that it needs prior knowledge of the signal, which hinders its application in practice. Xu [15, 16] suggested a new ehnrgram based on Envelope Harmonic-to-Noise Ratio (EHNR). The advantage of the EHNR lies in that it is insensitive to the large aperiodic impulses and can efficiently extract the interested periodic impulses at the same time. But the EHNR could also get into trouble since it is very sensitive to the harmonic components, such as the rotating frequency component and its higher order harmonics, of the vibration signal.

However, there are some issues still worthy of discussion. Generally, besides the interested fault related impulse components, real collected vibration signals also contain some interference, such as background noises and rotating frequency related harmonic components. In some cases, random impulses coming from external environment further complicates the bearing fault diagnostic problem.

In view of that, a new parameter, named Shock Pulse Index (SPI), is proposed in this paper. It combines the mutual advantages of both the kurtosis and the EHNR at the same time and can therefore accurately help extract the periodic impulses from the raw signal. Moreover, the SPI is insensitive to the aperiodic impulse and the rotating frequency related harmonics. This in turn improves the robustness of the diagnostic process. Here background noise is a non-ignorable factor that should be carefully considered. Maximum Correlated Kurtosis Deconvolution (MCKD) [17] is an effective approach to highlight the fault related periodic impulse components [18]. However, whether its parameter settings are proper or not has a direct influence on analysis results [19, 20]. Therefore, a new way of parameter optimization for the MCKD based on the SPI is then implemented to ensure correct extraction of interested information. Finally, considering the modulation characteristic of the faulty bearing signal [2], a nonlinear differential operator, Teager Energy Operator (TEO) [21, 22], is used to estimate the energy required to find the Fault Characteristic Frequency (FCF). The amplitude envelope and instantaneous frequency of any modulated signals then can be obtained.

The paper is arranged as follows: The theory of this research is stated in section 2. In section 3, the properties of the SPI are illustrated by simulation analysis. The method based on the SPI is proposed in section 4. The performance of the novel method is illustrated by real data in section 5. And finally, the conclusion is given in section 6.

2. Theoretical Background

2.1. Teager energy opertor

For a signal $x(t)$, the Teager energy operator Ψ is defined as [23-25]:

$$\Psi[x(t)] = \left(\frac{dx(t)}{dt}\right)^2 - x(t)\left(\frac{d^2x(t)}{dt}\right) = [\dot{x}(t)]^2 - x(t)\ddot{x}(t), \quad (1)$$

where $\dot{x}(t)$ and $\ddot{x}(t)$ are the first and the second derivative of $x(t)$ with respect to time t, respectively. The energy operator in Equation (1) is defined for continuous time signals. Using difference to approximate derivatives, its counterpart for discrete time signals $x(n)$ becomes

$$\Psi[x(n)] = [x(n)]^2 - x(n-1)x(n+1). \quad (2)$$

Preprints (www.preprints.org) | NOT PEER-REVIEWED | Posted: 20 January 2017 doi:10.20944/preprints201701.0091.v1

Peer-reviewed version available at Sensors 2017, 17, 535; doi:10.3390/s17030535

For a vibration displacement of the linear oscillator of undamped free vibration

$$x(t) = A\cos(2\pi ft + \varphi). \tag{3}$$

Its first and second derivatives, i.e. velocity and acceleration, are respectively

$$\dot{x}(t) = -2\pi Af\sin(2\pi ft + \varphi), \tag{4}$$

$$\ddot{x}(t) = -4\pi^2 Af^2\cos(2\pi ft + \varphi), \tag{5}$$

where A is the amplitude, f is the frequency, and φ is an initial phase.

Applying the Teager energy operator Ψ to the Equation (3) and substituting for its first and second derivatives by the $\dot{x}(t)$ and $\ddot{x}(t)$ from Equations (4) and (5), yields

$$\Psi[x(t)] = [\dot{x}(t)]^2 - x(t)\ddot{x}(t) = 4\pi^2A^2f^2. \tag{6}$$

Further applying the Teager energy operator Ψ to the derivative of $x(t)$, i.e. $\dot{x}(t)$, produces

$$\Psi[\dot{x}(t)] = [\ddot{x}(t)]^2 - \dot{x}(t)\dddot{x}(t) = 16\pi^4A^2f^4. \tag{7}$$

The absolute amplitude and the frequency can then be obtained from Equations (6) and (7) as follows:

$$|A| = \frac{\Psi[x(t)]}{\sqrt{\Psi[\dot{x}(t)]}}, \tag{8}$$

$$f = \frac{1}{2\pi}\sqrt{\frac{\Psi[\dot{x}(t)]}{\Psi[x(t)]}}. \tag{9}$$

This is what we called the TEO algorithm that can be generalized to signals with arbitrary time-varying amplitude and frequency. Thus the absolute value of instantaneous amplitude envelope $a(t)$ and the instantaneous frequency $f(t)$ can be estimated as:

$$|a(t)| = \frac{\Psi[x(t)]}{\sqrt{\Psi[\dot{x}(t)]}}, \tag{10}$$

$$f(t) = \frac{1}{2\pi}\sqrt{\frac{\Psi[\dot{x}(t)]}{\Psi[x(t)]}}. \tag{11}$$

If no special instructions, the envelope spectrum of this paper are generated by the TEO.

2.2. Maximum correlated kurtosis deconvolution

Inspired by the Minimum entropy deconvolution (MED) technique, an improved novel deconvolution technique named Maximum correlated kurtosis deconvolution (MCKD) was proposed [17]. The MCKD technique is that select a FIR filter to maximize the Correlated Kurtosis (CK), which takes advantage of the periodicity of the faults and requires no AR model stage prior to deconvolution, of the resulting signal which emphasizes high Kurtosis while encouraging periodicity about a specific period.

Consider a discrete signal $y(n)$ that is the response of the bearing excited by the fault impulses signal $x(n)$. The essence of the MCKD algorithm is that searches for a FIR filter $f(k)$ to maximize the CK of the signal $x(n)$ recovered from the input signal:

$$x(n) = \sum_{k=1}^{L} f(k)y(n-k+1), \tag{12}$$

where $f(k) = [f_1\ f_2 \cdots f_L]^T$, L is the length of the FIR filter.

The Correlated Kurtosis is defined as:

$$CK_M(T) = \frac{\sum_{n=1}^{N}\left(\prod_{m=0}^{M} x_{n-mT}\right)^2}{\left(\sum_{n=1}^{N} x_n^2\right)^{M+1}}, \tag{13}$$

where T is the period of impulses and M is the shift number.

The optimization function of the MCKD is expressed as:

$$MCKD_M(T) = \max_{f(k)} CK_M(T) = \max_{f(k)} \frac{\sum_{n=1}^{N}\left(\prod_{m=0}^{M} x_{n-mT}\right)^2}{\left(\sum_{n=1}^{N} x_n^2\right)^{M+1}}. \tag{14}$$

Preprints (www.preprints.org) | NOT PEER-REVIEWED | Posted: 20 January 2017 doi:10.20944/preprints201701.0091.v1

Peer-reviewed version available at Sensors 2017, 17, 535; doi:10.3390/s17030535

The above optimization problem is equivalent to solve Equation, as follows:

$$\frac{d}{df(k)} CK_M(T) = 0. \tag{15}$$

Solving the Equation (15) and the coefficients f(k) can be expressed by a matrix form as follows:

$$f(k) = \frac{\|\vec{x}\|^2}{2\|\vec{\beta}\|^2} (Y_0 Y_0^T)^{-1} \sum_{m=0}^{M} Y_{mT} \vec{\alpha}_m, \tag{16}$$

where $\vec{\alpha}_m = \begin{bmatrix} x_{1-mT}^{-1}(x_1^2 x_{1-T}^2 \cdots x_{1-MT}^2) \\ x_{2-mT}^{-1}(x_2^2 x_{2-T}^2 \cdots x_{2-MT}^2) \\ \vdots \\ x_{N-mT}^{-1}(x_N^2 x_{N-T}^2 \cdots x_{N-MT}^2) \end{bmatrix}$, $\vec{\beta} = \begin{bmatrix} x_1 x_{1-T} \cdots x_{1-MT} \\ x_2 x_{2-T} \cdots x_{2-MT} \\ \vdots \\ x_N x_{N-T} \cdots x_{N-MT} \end{bmatrix}$, $Y_{mT} = \begin{bmatrix} y_{1-mT} & y_{2-mT} & \cdots & y_{N-mT} \\ 0 & y_{1-mT} & \cdots & y_{N-1-mT} \\ \vdots & \vdots & \ddots & \vdots \\ 0 & 0 & \cdots & y_{N-L-mT+1} \end{bmatrix}_{L \times N}$.

Calculating the coefficients f(k) by Equation (16), the MCKD can extract the fault impulses from the vibration signal effectively.

2.3. Shock pulse index

2.3.1. Kurtosis

Kurtosis as the fourth standardized moment can reflects the distribution characteristics of vibration signals and it was defined as:

$$\text{Kurtosis}(x) = \frac{\int_{-\infty}^{+\infty} [x(t) - \bar{x}]^4 p(x)\, dx}{\sigma^4}, \tag{17}$$

where x(t) is the instantaneous of amplitude, $\bar{x}$ is the mean of amplitude, p(x) is the probability density and σ is the standard deviation.

As shown in Figure 1, Kurtosis is a measure of how outlier-prone a distribution is. The kurtosis of the normal distribution is 3. Distributions that are more outlier-prone than the normal distribution have kurtosis greater than 3; distributions that are less outlier-prone have kurtosis less than 3. Therefore, kurtosis can effectively identify the impulse signal from the vibration signal.

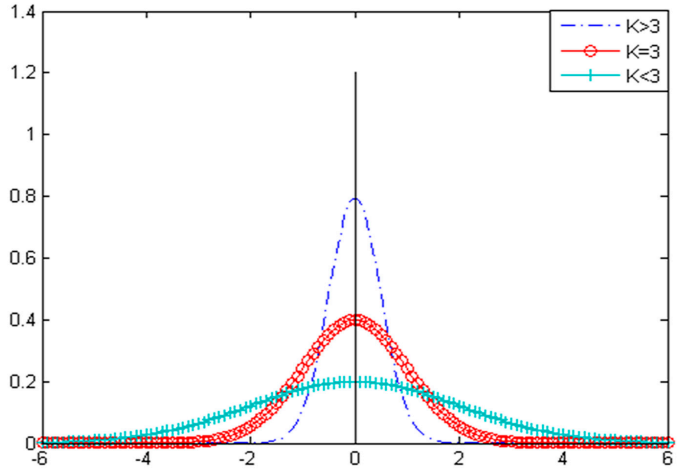

Figure 1. The outlier-prone of a distribution.

2.3.2. Envelope harmonic-to-noise ratio

The harmonic-to-noise ratio (HNR) is an important characteristic parameters and it is used to describe the ratio of harmonic and noise components in speech signal analysis. In view of the

Preprints (www.preprints.org) | NOT PEER-REVIEWED | Posted: 20 January 2017 doi:10.20944/preprints201701.0091.v1

Peer-reviewed version available at Sensors 2017, 17, 535; doi:10.3390/s17030535

fault-induced periodic impulses are usually modulated at resonance frequencies, the EHNR was proposed to eliminate the phenomenon of modulation [15, 16]. The EHNR algorithm can be calculated as follows:

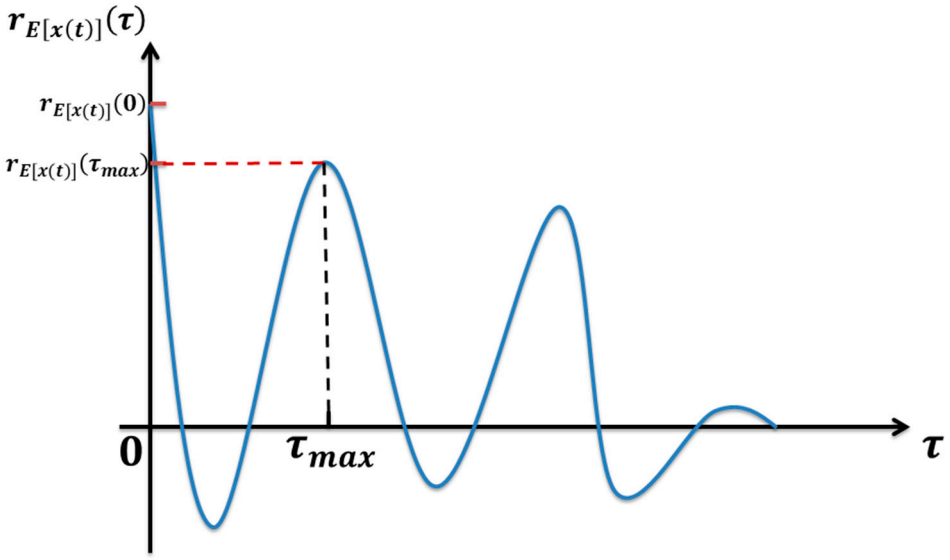

Figure 2. The autocorrelation function of the $\mathbf{r_{E[x(t)]}(\tau)}$.

Obtain the envelope signal E[x(t)] by Hilbert transform of the measured signal x(t) and remove the DC component.

$$x'(t) = H\{x(t)\} = \frac{1}{\pi}\int_{-\infty}^{+\infty}\frac{x(\tau)}{t-\tau}d\tau, \quad (18)$$

$$E[x(t)] = \sqrt{x^2(t) + x'^2(t)}, \quad (19)$$

$$E[x(t)] = E[x(t)] - \text{mean}\{E[x(t)]\}. \quad (20)$$

Computing the autocorrelation of E[x(t)].

$$r_{E[x(t)]}(\tau) = \int E[x(t)]\,E[x(t+\tau)]\,dt. \quad (21)$$

Then the EHNR can be represented as:

$$\text{EHNR} = \frac{r_{E[x(t)]}(\tau_{max})}{r_{E[x(t)]}(0) - r_{E[x(t)]}(\tau_{max})}, \quad (22)$$

where τ is delay time, τ_{max} is the delay time of the maximum of autocorrelation function in addition to the zero point, the point indicated in Figure 2, $x'(t)$ is the Hilbert transform of the $x(t)$, $E[x(t)]$ is the amplitude of the Hilbert transform, $r_{E[x(t)]}(\tau)$ is the autocorrelation function of the $E[x(t)]$.

2.3.3. Shock pulse index

As the characteristic parameter of vibration signal, kurtosis can reflects the shock characteristic of vibration signal, but the only fly in the ointment is that it is easily influenced by background noise and larger aperiodic impulse. On the other hand, the EHNR, as a new characteristic parameter of vibration signal, can indicates the ratio of harmonic and noise component in vibration signal and that is a good characteristic parameter but interfered by other harmonic component such as rotating frequency. Inspired by these two parameters, the SPI that absorbs the advantages and abandons the disadvantages of both two indexes was proposed.

According to the dynamic model of the REB [15, 26], the vibration signal of the REB usually consists of four parts i.e. the periodic impulses, the vibration components from related rotating

Preprints (www.preprints.org) | NOT PEER-REVIEWED | Posted: 20 January 2017 doi:10.20944/preprints201701.0091.v1

Peer-reviewed version available at Sensors 2017, 17, 535; doi:10.3390/s17030535

parts, the aperiodic impulses from extraneous sources (large random impulses) and the background noise. The formula as shown:

$$x(t) = \sum_i A_i s(t - T_i) + \sum_j B_j s(t - T_j) + \sum_k C_k \cos(2\pi f_k t + \varphi_k) + n(t), \quad (23)$$

$$s(t) = e^{-\alpha t} \sin(2\pi f_r t), \quad (24)$$

where A_i is the amplitude of the ith impulse and T_i is the time of its occurrence for the periodic impulses, B_j is the amplitude of the jth impulse and T_j is the time of its occurrence for the aperiodic impulses, C_k, f_k and φ_k are the amplitude, frequency and initial phase of the related rotating parts, respectively. $n(t)$ is the background noise. α is the coefficient of resonance damping, f_r is the resonance frequency.

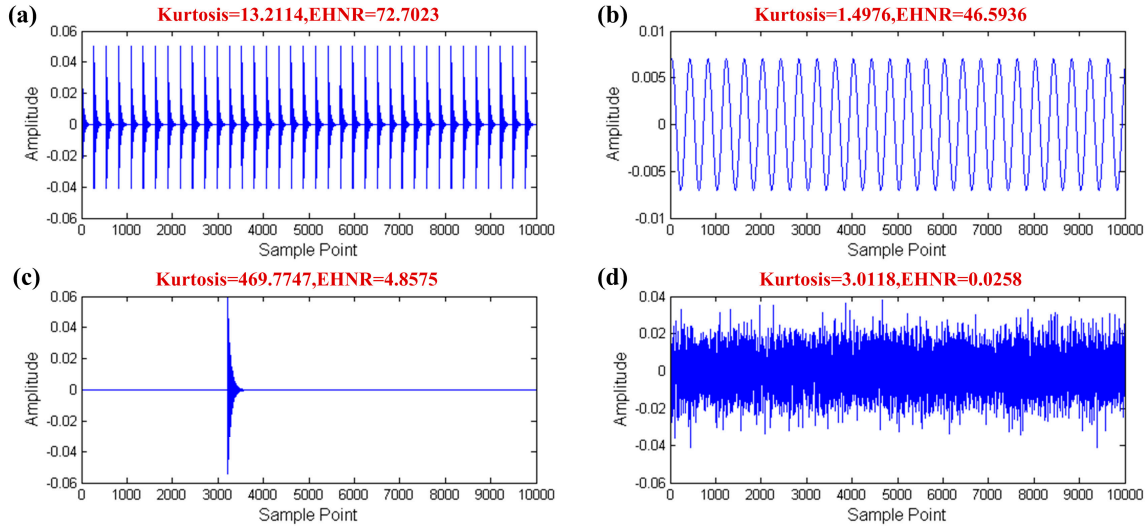

Figure 3. The simulation data of the four parts of the REB vibration signal: (a) fault impulses; (b) other rotating component; (c) aperiodic impulse; (d) white noise.

As Figure 3 shown, creating the simulation signals of the four parts of the REB vibration signal and calculating the kurtosis and the EHNR values, respectively. The fault impulses with the high kurtosis and EHNR value meanwhile, other rotating component only with the high EHNR value, the aperiodic impulse only with the high kurtosis value and the kurtosis and the EHNR value of the white noise are all not high are shown in Figure 3. Therefore the fault impulses of the REB has two characteristics i.e. impulsive and periodic at the same time and single kurtosis or EHNR index cannot be comprehensively summarized its physical characteristic. The organic fusion of the kurtosis and the EHNR, the SPI was put forward as follows:

$$SPI = \log_2(1 + a * kurtosis + b * EHNR) \quad (25)$$

where a and b are weight coefficient of the kurtosis and the EHNR, respectively. 0.6 and 0.4 is recommended values of a and b. The kurtosis and the EHNR are all normalized values.

3. Properties of the SPI

3.1. Capability of distinguishing fault information under high background noise

As a part of the test signal, background noise is inevitable and it directly affects the final diagnosis. Therefore it is an important ability of characteristic parameter to distinguish the fault information under the high background noise. A simulation is given here to illustrate the capability of the SPI to distinguish the fault information under the high background noise. In this simulation data, sampling frequency is 20000Hz, sampling points is 20480, impulse amplitude is 0.03, the coefficient of resonance damping is 620, resonance frequency is 5800Hz, the FCF is 74Hz, the mean and standard deviation of white noise are 0 and 1, respectively. The fault impulses without other components is shown in Figure 4(a). Here, strong white noise is shown in Figure 4(b) and Figure 4(c)

Preprints (www.preprints.org) | NOT PEER-REVIEWED | Posted: 20 January 2017 doi:10.20944/preprints201701.0091.v1

Peer-reviewed version available at Sensors 2017, 17, 535; doi:10.3390/s17030535

shows the mixed signal of the fault impulses and the white noise. With the aid of Fast-gram technique [12], using the mixed signal to test the antinoise ability of three parameters.

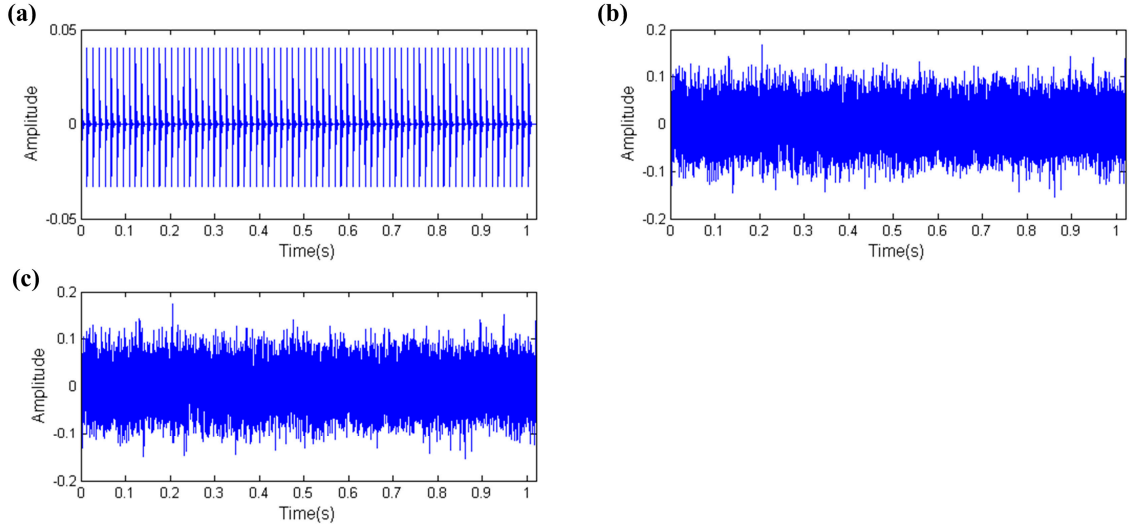

Figure 4. The simulation signal of the REB (including fault impulses and white noise): (a) fault impulses; (b) white noise; (c) mixed signal.

The result of Fast kurtogram is shown in Figure 5(a). As is shown in the figure, the yellow dotted box is filter band, which the center frequency equals 104.1667Hz and has a large gap with the resonance frequency (5800Hz). The filtered signal is shown in Figure 5(b) and Figure 5(c) shows the envelope spectrum of the filtered signal. From Figure (5), it is obvious that the Fast kurtogram loses effectiveness under strong white noise and the FCF is completely submerged by noise. The result of the Fast ehnrgram and the Fast spigram are shown in Figure 6(a) and 6(b). These two techniques that select the same center frequency (5859.375Hz) and bandwidth (156.25Hz) of filter are shown in the yellow dotted boxes. Moreover the center frequency is nearly equal to the resonance frequency, therefore it shows that the filter band is the optimal band. The filtered signal and its envelope spectrum are shown in Figure 6(c) and 6(d), respectively. The FCF is accurately found in the envelope spectrum of the filtered signal.

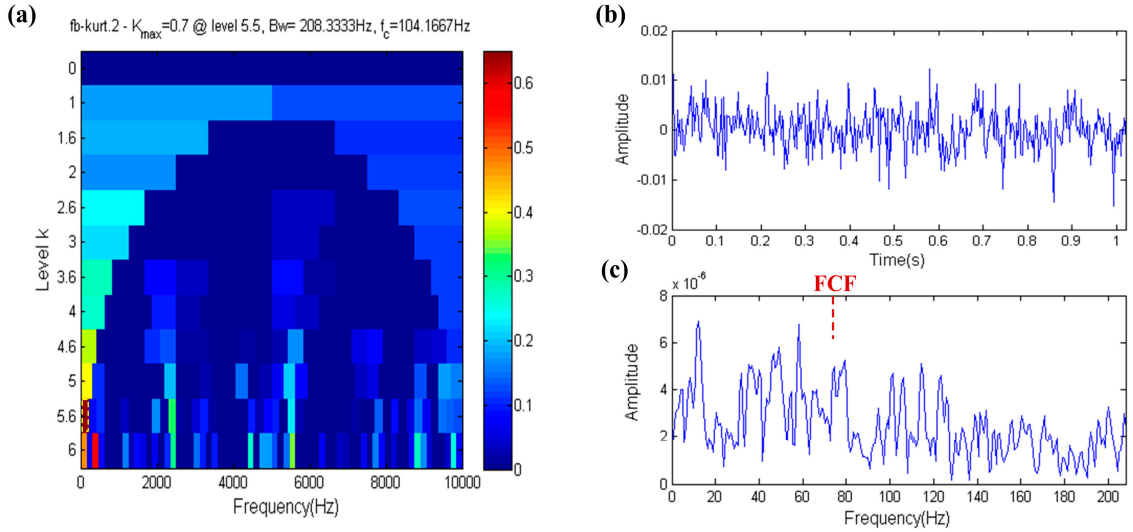

Figure 5. Fast-gram based on the kurtosis: (a) Fast kurtogram; (b) the filtered signal; (c) the envelope spectrum of (b).

Preprints (www.preprints.org) | NOT PEER-REVIEWED | Posted: 20 January 2017 doi:10.20944/preprints201701.0091.v1

Peer-reviewed version available at Sensors 2017, 17, 535; doi:10.3390/s17030535

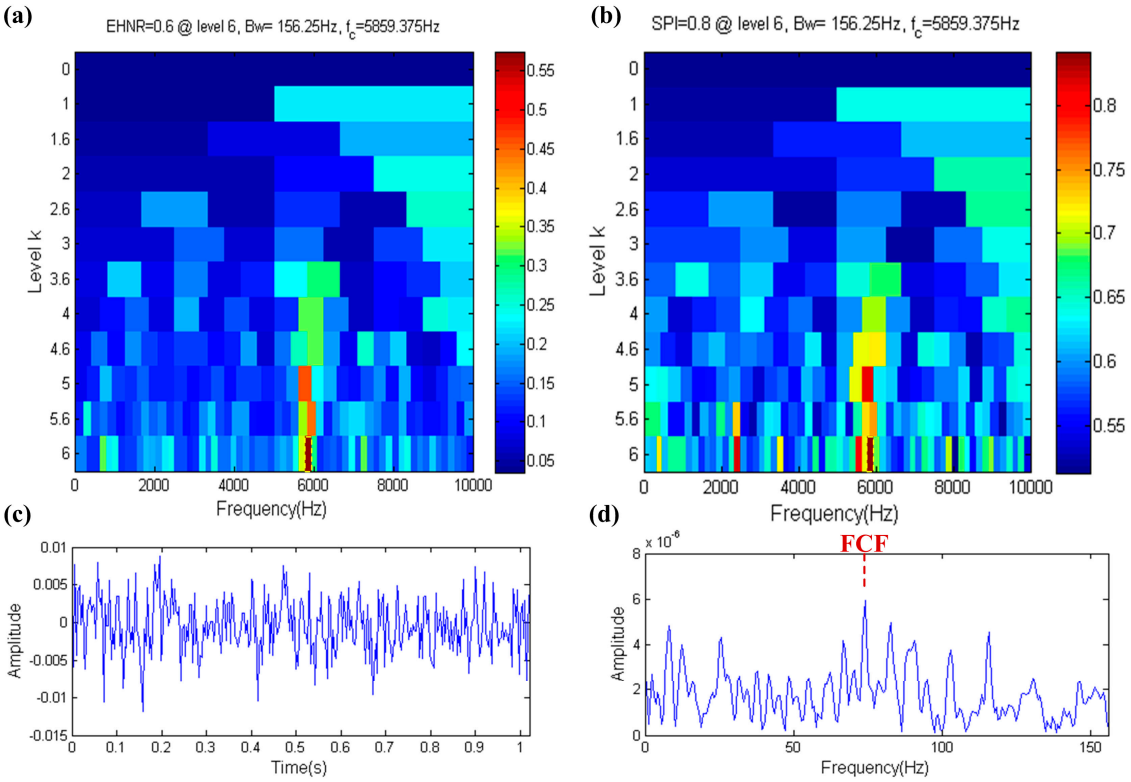

Figure 6. Fast-gram based on the EHNR and the SPI: (a) Fast ehnrgram; (b) Fast spigram; (c) the filtered signal; (d) the envelope spectrum of (c).

3.2. Capability of distinguishing fault impulses and other harmonic component

Harmonic component, such as rotating frequency, is an important part of the vibration signal of the rotating machinery. The energy of rotating frequency of the shaft is usually small in the vibration signal of rotating machinery that the REB is the core component, so the rotating frequency does not affect the extraction of the fault impulses of the REB under normal circumstances. However the energy of the rotating frequency is close to the energy of fault impulses when the REB is in the stage of early failure or shaft failure occurs. At this time, identification of the fault impulses of the REB will be affected by the interference of the rotating frequency.

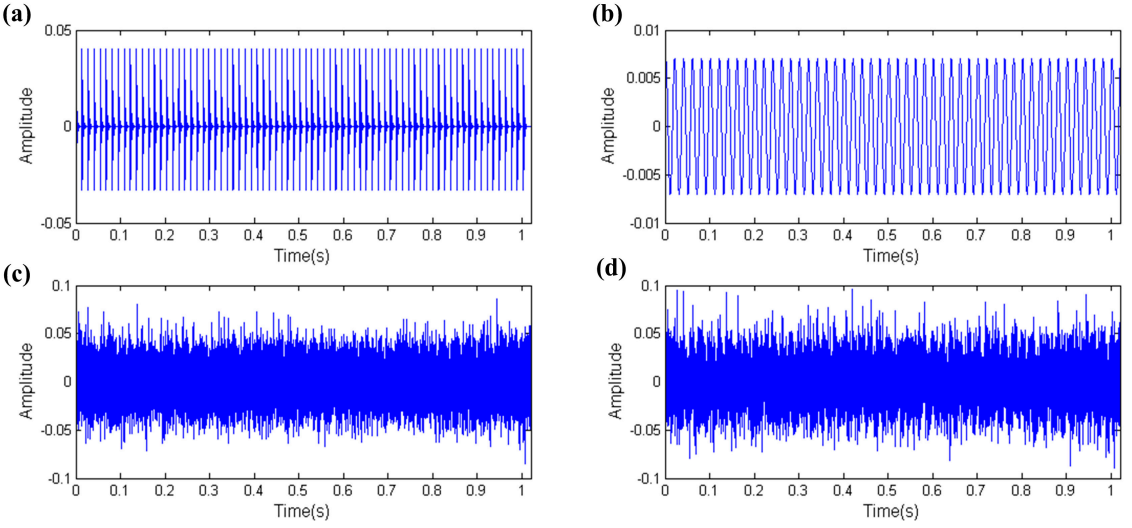

Figure 7. The simulation signal of the REB (including fault impulses, harmonic component and white noise): (a) fault impulses; (b) harmonic component; (c) white noise; (d) mixed signal.

Preprints (www.preprints.org) | NOT PEER-REVIEWED | Posted: 20 January 2017 doi:10.20944/preprints201701.0091.v1

Peer-reviewed version available at Sensors 2017, 17, 535; doi:10.3390/s17030535

On the basis of the simulation signal of section 3.1, adding a harmonic component that the frequency and amplitude are 50Hz and 0.007 respectively and reducing the strength of noise so as to make the harmonic component become a single test index. The simulation signal is shown in Figure 7. The periodic fault impulses, the harmonic component, the white noise and the mixed signal are shown in Figure 7(a), (b), (c) and (d) , respectively. Then testing the capability of distinguishing fault impulses and other harmonic component of these three indexes in accordance with the thinking of section 3.1.

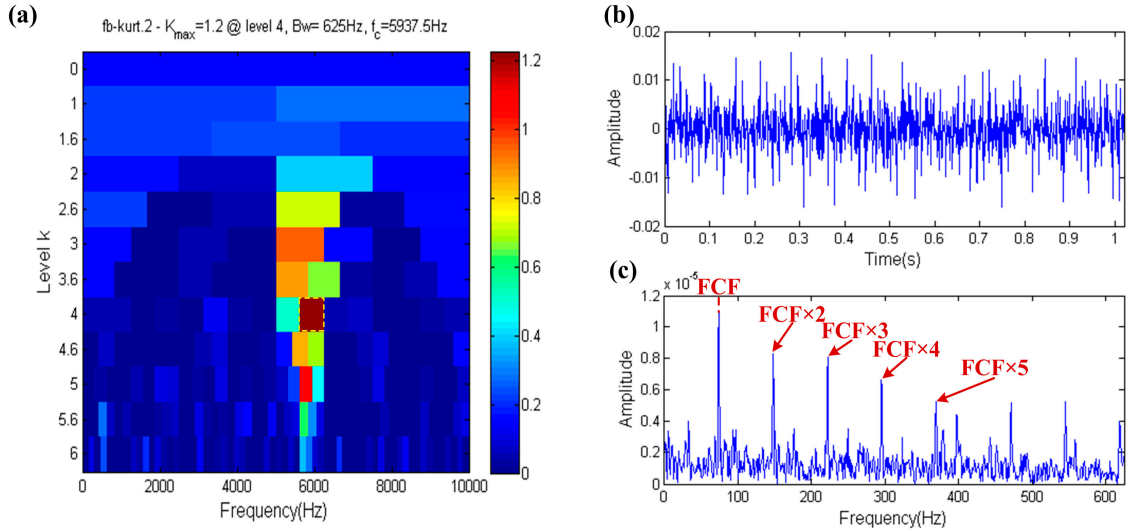

Figure 8. Fast-gram based on the kurtosis: (a) Fast kurtogram; (b) the filtered signal; (c) the envelope spectrum of (b).

The result of Fast kurtogram technique is shown in Figure 8, Fast kurtogram selects the filter band that center frequency and bandwidth are 5937.5Hz and 625Hz respectively, which is shown in the yellow dotted box in Figure 8(a). The center frequency is close to the resonance frequency, so this means that Fast kurtogram can accurately identify the fault. The periodic impulses obviously occur in the filtered signal in Figure 8(b) and its envelope spectrum indicates more clearly harmonics even at high order harmonics of the FCF, which is shown in Figure 8(c). Hence, kurtosis index has the ability to resist the interference of harmonic component.

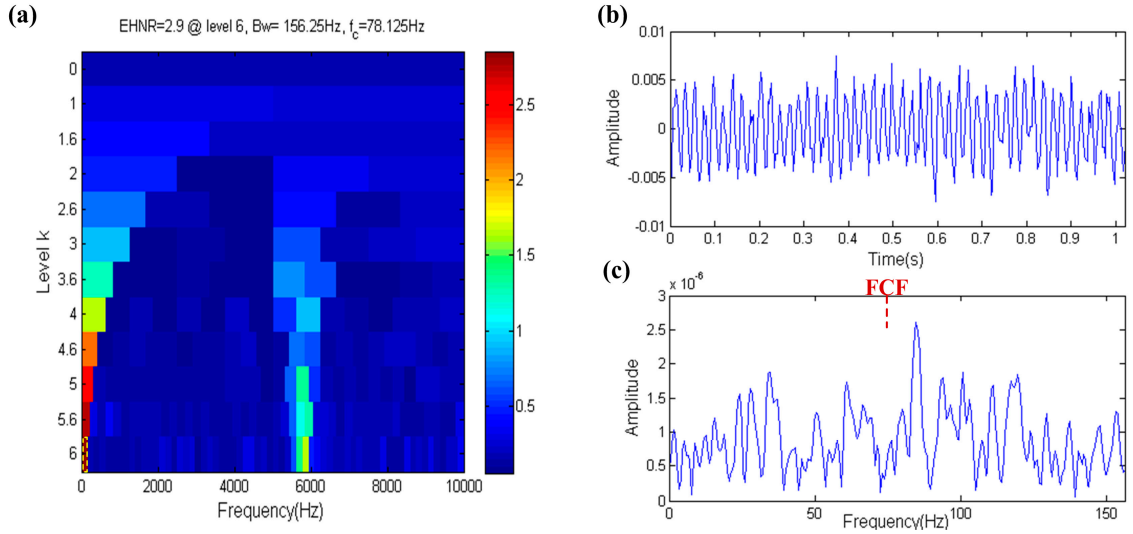

Figure 9. Fast-gram based on the EHNR: (a) Fast ehnrgram; (b) the filtered signal; (c) the envelope spectrum of (b).

The result of Fast ehnrgram technique is shown in Figure 9, the filter band that the center frequency and bandwidth are 78.125Hz and 156.25Hz respectively is selected by Fast ehnrgram,

Preprints (www.preprints.org) | NOT PEER-REVIEWED | Posted: 20 January 2017 doi:10.20944/preprints201701.0091.v1

Peer-reviewed version available at Sensors 2017, 17, 535; doi:10.3390/s17030535

which is shown in the yellow dotted box in Figure 9(a). There is a large gap between the center frequency and the resonance frequency, this is due to the EHNR index is influenced by the low frequency harmonic component. The waveform of the filtered signal is almost like a harmonic signal in Figure 9(b) and it is distinct from the fault signal. Moreover the envelope spectrum of the filtered signal cannot indicates the FCF, which is shown in Figure 9(c). Therefore the EHNR index is easily influenced by harmonic component.

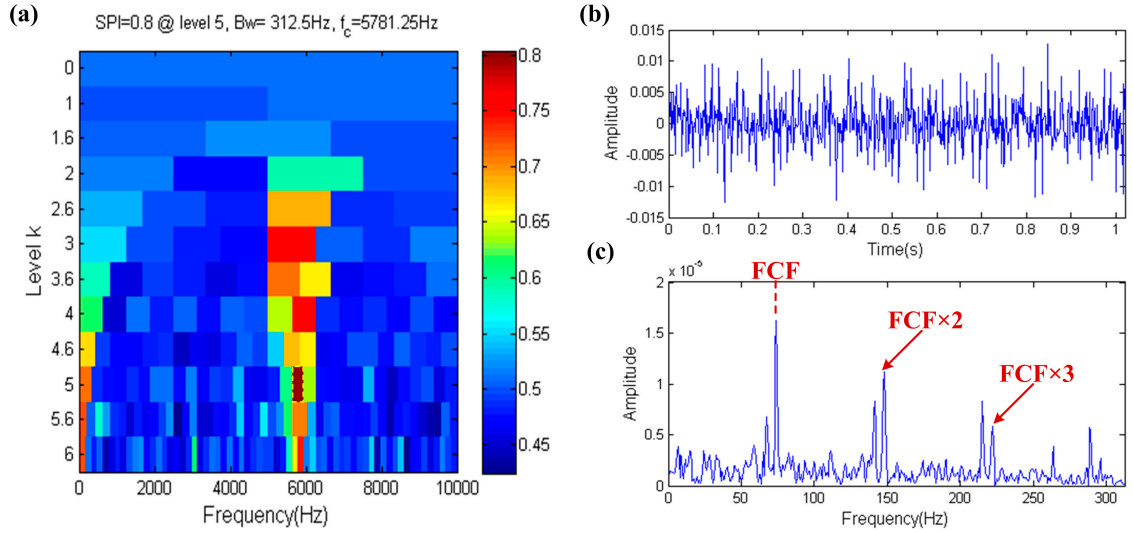

Figure 10. Fast-gram based on the SPI: (a) Fast spigram; (b) the filtered signal; (c) the envelope spectrum of (b).

The result of Fast spigram technique is shown in Figure 10, the filter band that the center frequency and bandwidth are 5781.25Hz and 312.5Hz respectively is selected by Fast spigram, which is shown in the yellow dotted box in Figure 10(a). It is observed that the center frequency is close to the resonance frequency, so this means that Fast spigram can accurately identify the fault. The filtered signal is shown in Figure 10(b) and its waveform has obviously periodic impulses, the envelope spectrum of the filtered signal further proves the effectiveness of Fast spigram because the FCF and its high order harmonics are shown clearly in the envelope spectrum, which is shown in Figure 10(c). Therefore the SPI, like kurtosis, also has the ability to resist the interference of harmonic component.

3.3. Capability of distinguishing fault impulses and aperiodic impulse

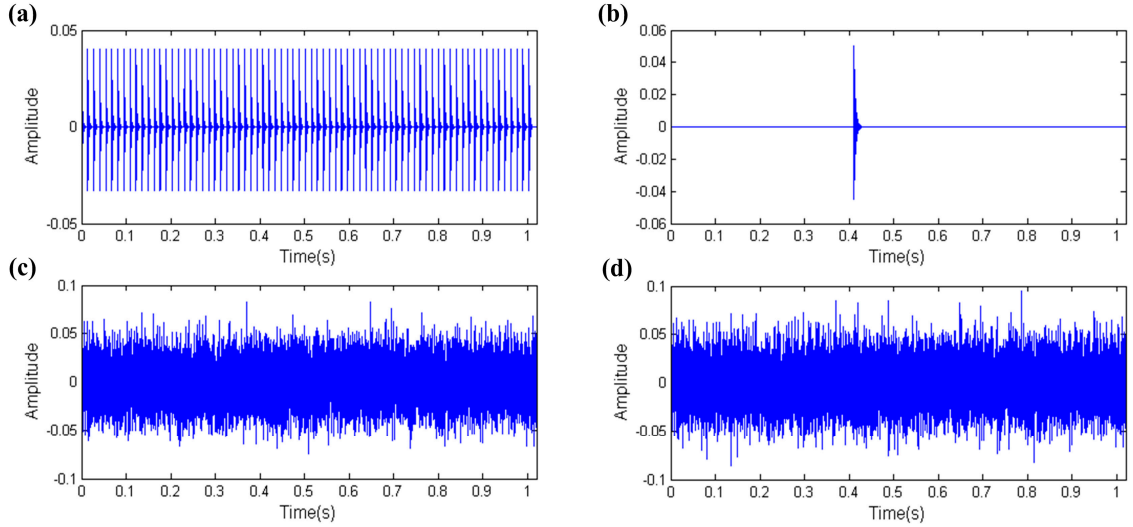

Figure 11. The simulation signal of the REB (including fault impulses, aperiodic impulse and white noise): (a) Fault impulses; (b) aperiodic impulse; (c) white noise; (d) mixed signal.

Preprints (www.preprints.org) | NOT PEER-REVIEWED | Posted: 20 January 2017 doi:10.20944/preprints201701.0091.v1

Peer-reviewed version available at Sensors 2017, 17, 535; doi:10.3390/s17030535

Aperiodic impulse, as a random impulse, may be due to random knock on the test rig or electricity interference and it is not common in the vibration signal of the REB, hence it is usually ignored. However once when it occurs, aperiodic impulse can produce the great interference to the diagnosis of the REB, therefore it is an important content of the REB fault diagnosis to accurately distinguish the aperiodic impulse and the fault impulse.

Using the thought of section 3.1 just like section 3.2, adding the aperiodic impulse that its resonance frequency and amplitude are 8700Hz and 0.05 respectively in the simulation signal, moreover reducing the strength of noise so as to make the aperiodic impulse become a single test index. Figure.11 shows the simulation signal. The periodic fault impulses, the aperiodic impulse, the white noise and the mixed signal are shown in Figure 11(a) ,(b),(c) and (d), respectively.

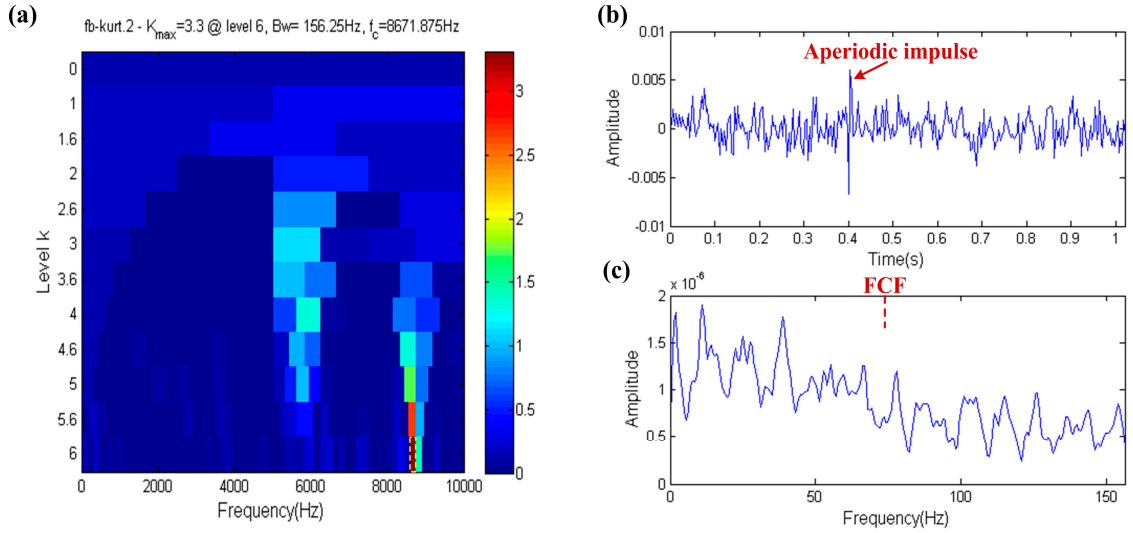

Figure 12. Fast-gram based on the kurtosis: (a) Fast kurtogram; (b) the filtered signal; (c) the envelope spectrum of (b).

The result of Fast kurtogram technique is shown in Figure 12, Fast kurtogram selects the filter band that the center frequency and bandwidth are 8671.875Hz and 156.25Hz respectively, which is shown in the yellow dotted box in Figure 12(a). The center frequency of filter band is close to the resonance frequency of the aperiodic impulse, which means that the diagnosis technology based on kurtosis is easily affected by the aperiodic impulse. In Figure 12(b), a large aperiodic impulse appears at about 0.4 second and the aperiodic impulse occurs at the same moment in the raw simulation signal, thus it is shown that the filtered signal only manifests the information of the aperiodic impulse and does not show the failure information. The same conclusion can be obtained in Figure 12(c), the FCF cannot be indicated in the envelope spectrum. Therefore, kurtosis index is vulnerable when it deals with the aperiodic impulse.

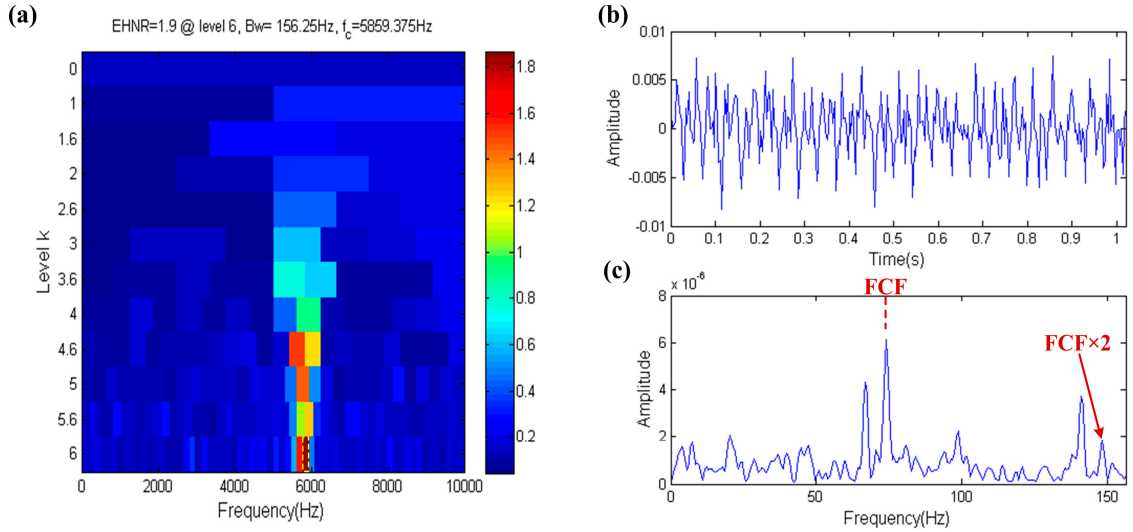

Preprints (www.preprints.org) | NOT PEER-REVIEWED | Posted: 20 January 2017 doi:10.20944/preprints201701.0091.v1

Peer-reviewed version available at Sensors 2017, 17, 535; doi:10.3390/s17030535

Figure 13. Fast-gram based on the EHNR: (a) Fast ehnrgram; (b) the filtered signal; (c) the envelope spectrum of (b).

The result of Fast ehnrgram technique is shown in Figure 13, the filter band that the center frequency and bandwidth are 5859.375Hz and 156.25Hz respectively, which is shown in the yellow dotted box in Figure 13(a). The center frequency of filter band is close to the resonance frequency of the fault impulses, that is to say the FCF should be indicated in the envelope spectrum. In Figure 13(b), the waveform of the filtered signal has obvious fault impulses and its envelope spectrum also indicates the FCF in Figure 13(c). Therefore, the EHNR index able to eliminate the impact of aperiodic impulse.

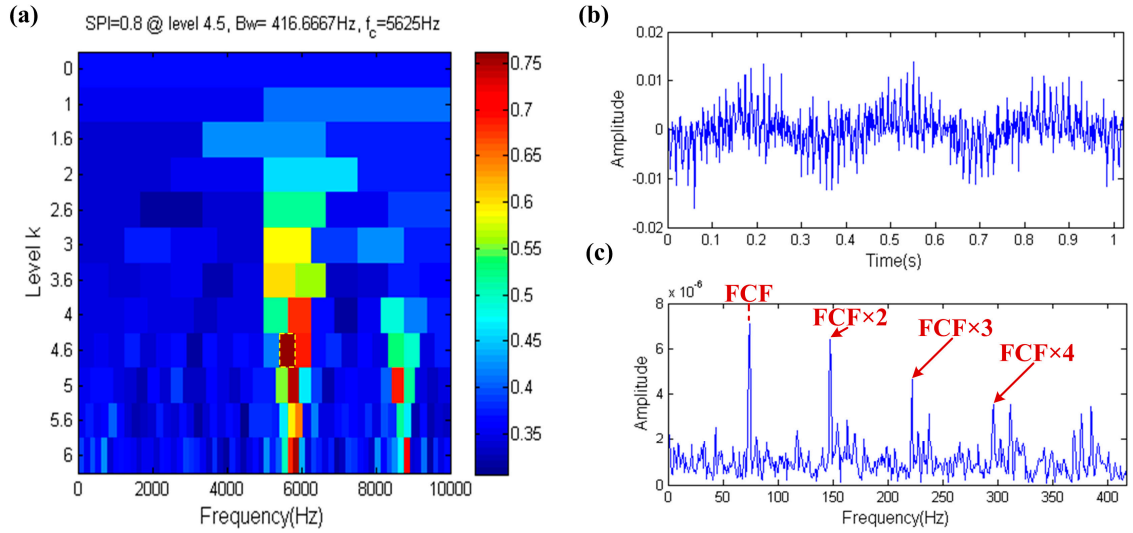

Figure 14. Fast-gram based on the SPI: (a) Fast spigram; (b) the filtered signal; (c) the envelope spectrum of (b).

The result of Fast spigram technique is shown in Figure 14, the filter band that the center frequency and bandwidth are 5625Hz and 416.6667Hz respectively, which is shown in the yellow dotted box in Figure 14(a). The center frequency of filter band is also close to the resonance frequency of the fault impulses just like Figure 13(a), so the same conclusion can be obtained. The filtered signal is shown in Figure 14(b) and its envelope spectrum obviously shows the FCF even at high order harmonics of the FCF in Figure 14(c). Therefore, the SPI index also has the ability to resist the interference of aperiodic impulse.

Through the simulation experiment, the performance of three parameters are tested under the interference of the strong noise, the harmonic component and the aperiodic impulse, respectively. The result of the simulation experiment can be concluded as follows:

1. Kurtosis index has the ability to resist the interference of the harmonic component, but it is not robust when deals with the interference of the strong noise and the aperiodic impulse.
2. The EHNR index can effectively eliminate the influence of the strong noise and the aperiodic impulse, however the harmonic component will disable it.
3. The SPI index keeps good ability to identify the fault impulse when it is in the face of the interference of the strong noise, the harmonic component or the aperiodic impulse.

In short, the fault diagnosis technology based on the SPI index can be applied to the fault diagnosis of the REB.

4. The proposed method for bearing fault diagnosis

The fault impulses of the REB can not only be modulated, but also convoluted with the system transfer function in the process of transfer, hence deconvolution is always an important part of the fault diagnosis of the REB. The MCKD, as an powerful deconvolution technique, has been used in some applications of the fault diagnosis of the REB and a set of appropriate preset parameters can

Preprints (www.preprints.org) | NOT PEER-REVIEWED | Posted: 20 January 2017 doi:10.20944/preprints201701.0091.v1

Peer-reviewed version available at Sensors 2017, 17, 535; doi:10.3390/s17030535

make it play a better effect. This paper proposed the method, which using the SPI as the index of the preset parameters optimization of the MCKD and combining with the TEO demodulation technology. So concrete steps as follows:

step1. Load the raw vibration signal measured by the accelerometer and calculate the theoretical fault characteristic frequency $f = \{f_o, f_e, f_c, f_i\}$ by using the geometrical parameters of the REB, then compute the period of impulses T through formula $T = f_s/f$. Where f_o, f_e, f_c and f_i are the fault characteristic frequencies of outer race, rolling element, cage and inner race, respectively, f_s is the sampling frequency.

step2. Set 100 as the lower limit, 500 as the upper limit and 20 as the step size for L; Set 1 as the lower limit, 7 as the upper limit and 1 as the step size for M; Then calculate the SPI value of the results of different preset parameters and find out the maximum of the SPI value. Next, use the maximum of the SPI value corresponding to the preset parameters as the MCKD's optimization parameters.

step3. Use the optimization parameters as the preset parameters of the MCKD to filter the raw signal, then obtain the envelope spectrum with the help of the TEO technique.

step4. Diagnose the failure type on the basis of the extracted characteristic frequency information from the envelope spectrum.

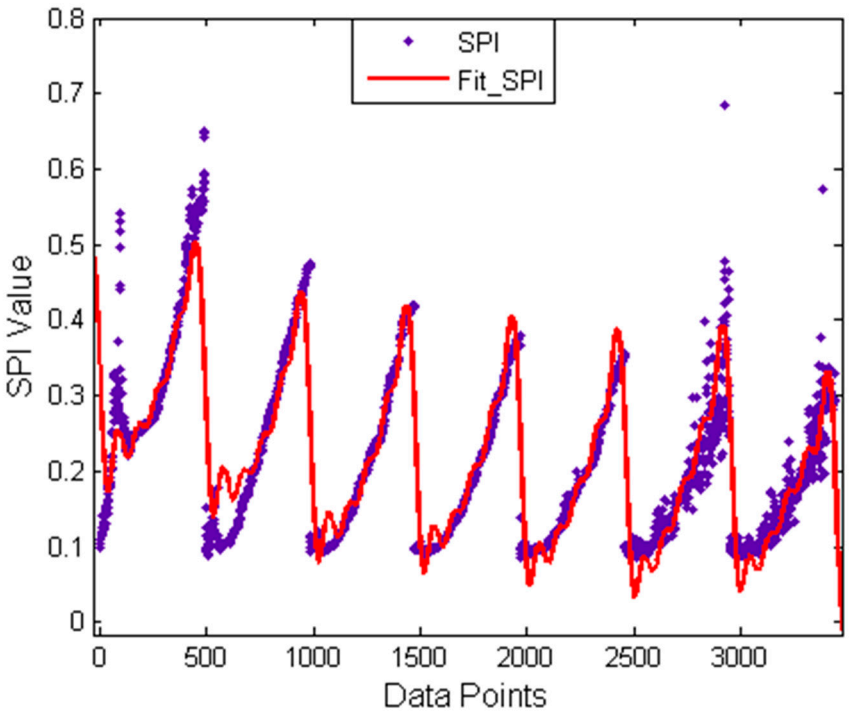

Figure 15. Trend curve of the SPI value.

In step2, the proposed method simplifies the preset parameters optimization of the MCKD. This is because a smaller L is not enough to effectively play the role of the MCKD and a smaller step size cannot significantly increase the precision of the solutions but can greatly reduce computational efficiency. The SPI value's trend of a set of real data is shown in Figure 15, figure in the purple dot is actual data distribution, while red line is the fitting curve of the actual data distribution and the type of fit is Sum of Sin Functions. In this test, setting 10 as the lower limit and 1 as the step size for L moreover the upper limit of L and the range of values of M consistent with the proposed method. From this figure, the SPI is roughly dispersed in seven areas and each area generally concentrates on a curve. What's more these seven areas just correspond to seven different M values, that is to say the SPI generally presents the monotone increasing tendency when M value remains the same and Fit_SPI curve further proves this

Preprints (www.preprints.org) | NOT PEER-REVIEWED | Posted: 20 January 2017 doi:10.20944/preprints201701.0091.v1

Peer-reviewed version available at Sensors 2017, 17, 535; doi:10.3390/s17030535

conclusion. Therefore it is scientific and effective for the simplification of the proposed method to quickly find the appropriate optimization parameters.

5. Experimental study for bearing fault diagnosis

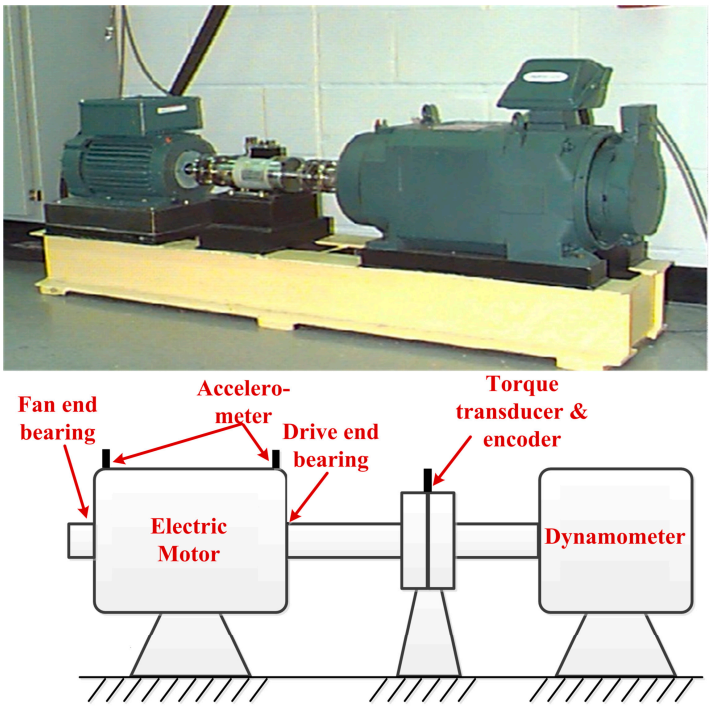

Figure 16. Overview of test bench and its structure diagram.

The real data comes from Case Western Reserve University (CWRU) Bearing Data Center [27]. The test bench and its structure diagram are shown in Figure 16, the test bench consists of a 2 horsepower motor, a torque transducer & encoder, a dynamometer and control electronics (not shown). Two bearings, Drive end bearing and Fan end bearing, are installed in both ends of motor shaft to support motor shaft itself. Drive end bearing (6205-2RS JEM SKF) and Fan end bearing (6203-2RS JEM SKF) are both deep groove ball bearing, moreover these two bearings are seeded with faults, which ranging from 0.007 inches to 0.040 inches in diameter are introduced separately at the inner raceway, rolling element and outer raceway using electro-discharge machining. Faulted bearings are reinstalled into the test motor and vibration data is recorded for motor loads of 0 to 3 horsepower, moreover the motor speeds ranges 1796 from 1728 RPM. Accelerometers are attached to the housing with magnetic bases and are placed at the 12 o'clock position at both the Drive end and Fan end of the motor housing. Vibration signals, which are post processed in a Matlab environment are collected using a 16 channel DAT recorder. Vibration data is collected at 12000 and 48000 samples per second for Drive end bearing, moreover speed and horsepower data are collected using the torque transducer & encoder and are recorded by hand. In this study, the test data are all collected at 12000 samples per second for Drive end bearing and the inner raceway, rolling element and outer raceway fault data are random taken a set of data for testing, respectively.

5.1. Outer raceway fault diagnosis

The selection of the outer raceway fault data is OR021@12_1 and intercepting 5120 data points

Preprints (www.preprints.org) | NOT PEER-REVIEWED | Posted: 20 January 2017 doi:10.20944/preprints201701.0091.v1

Peer-reviewed version available at Sensors 2017, 17, 535; doi:10.3390/s17030535

from 50001th point to 55120th point in order to improve computational efficiency in original data. The load is 1 horsepower and opposites to the sensor. What's more, the speed of motor is 1771RPM, the bearing defect size is 0.021 inches and the theoretical outer raceway fault characteristic frequency is 105.81Hz. The result of signal processing through the proposed method is shown in Figure 17.

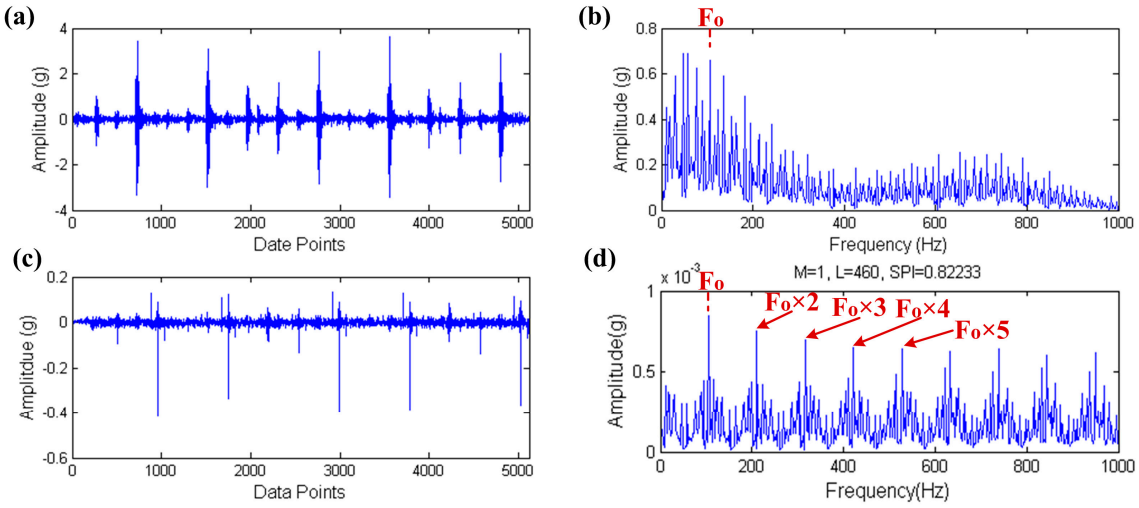

Figure 17. The result of outer raceway fault diagnosis: (a) the raw signal; (b) the envelope spectrum of (a); (c) the filtered signal; (d) the envelope spectrum of (c).

Due to the theoretical fault characteristic frequencies of the REB are all not high (about 100Hz to 200Hz), so showing the former 1000Hz frequency band is enough for the envelope spectrum. The whole study uses this thought and what follows need not to repeat. Input signal and its envelope spectrum are shown in Figure 17(a) and 17(b). Although the outer raceway fault characteristic frequency Fo is found in the envelope spectrum of the input signal, it is not highlight and other components almost submerge it. Therefore, the envelope spectrum of the input signal cannot indicate the fault clearly. The filtered signal, which is processed by the proposed method is shown in Figure 17(c) and its envelope spectrum is shown in Figure 17(d). Fo is clearly found in the envelope spectrum even at high order harmonic, that is to say bearing fault can be easily found after the processing of the proposed method.

5.2. Inner raceway fault diagnosis

The selection of the inner raceway fault data is IR014_3 and intercepting 5120 data points from 60001th point to 65120th point in order to improve computational efficiency in original data. The load is 3 horsepower. What's more, the speed of motor is 1728RPM, the bearing defect size is 0.014 inches and the theoretical inner raceway fault characteristic frequency is 155.96Hz. The result of signal processing through the proposed method is shown in Figure 18.

The input signal and its envelope spectrum are shown in Figure 18(a) and 18(b). The inner raceway fault characteristic frequency Fi is also found in the envelope spectrum of the input signal like section 5.1, however Fi is not obvious in multitudinous spectral lines and it is not easy to find it. The filtered signal, which is processed by the proposed method is shown in Figure 18(c) and its envelope spectrum is shown in Figure 18(d). In Figure 18(d), Fi and its high order harmonics are clearly highlighted in the envelope spectrum, this means that the inner raceway fault also can be easily found after the processing of the proposed method.

Preprints (www.preprints.org) | NOT PEER-REVIEWED | Posted: 20 January 2017 doi:10.20944/preprints201701.0091.v1

Peer-reviewed version available at Sensors 2017, 17, 535; doi:10.3390/s17030535

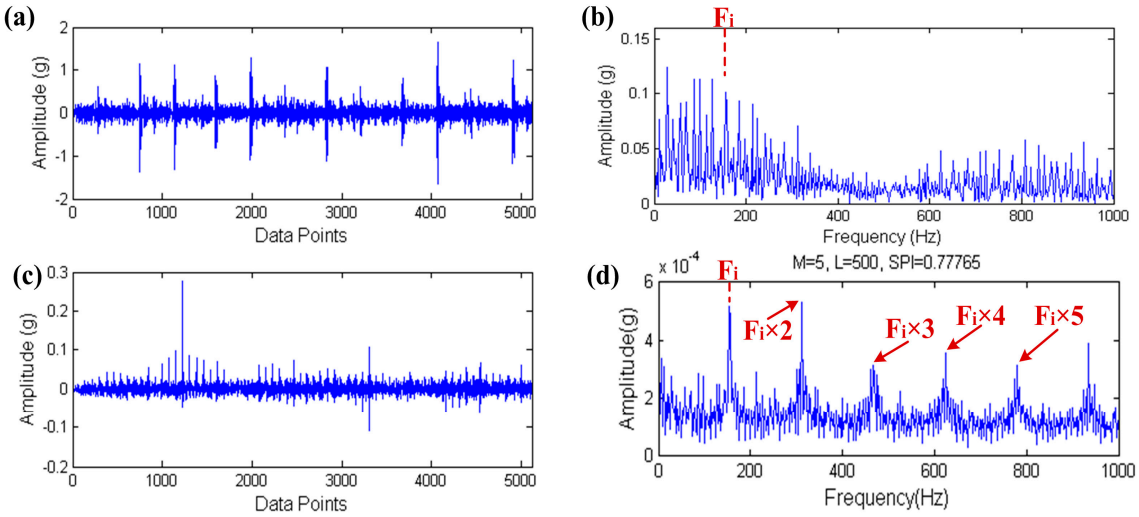

Figure 18. The result of inner raceway fault diagnosis: (a) the raw signal; (b) the envelope spectrum of (a); (c) the filtered signal; (d) the envelope spectrum of (c).

5.3. Rolling element fault diagnosis

The selection of the rolling element fault data is B021_0 and intercepting 5120 data points from 70001th point to 75120th point in order to improve computational efficiency in original data. The load is 0 horsepower. What's more, the speed of motor is 1796RPM, the bearing defect size is 0.021 inches and the theoretical rolling element fault characteristic frequency is 141.09Hz. The result of signal processing through the proposed method is shown in Figure 19.

The input signal and its envelope spectrum are shown in Figure 19(a) and 19(b), respectively. In the envelope spectrum of the input signal, the outer and inner raceway fault characteristic frequency Fo and Fi are both found, however the rolling element fault characteristic frequency Fe is submerged by multitudinous spectral lines, moreover Fo and Fi are both not highlighted because of the interference of other spectral lines. The filtered signal and its envelope spectrum are shown in Figure 19(c) and 19(d), respectively. Through the processing of the proposed method, Fe and its high order harmonics are obviously found in the Figure 19(d).

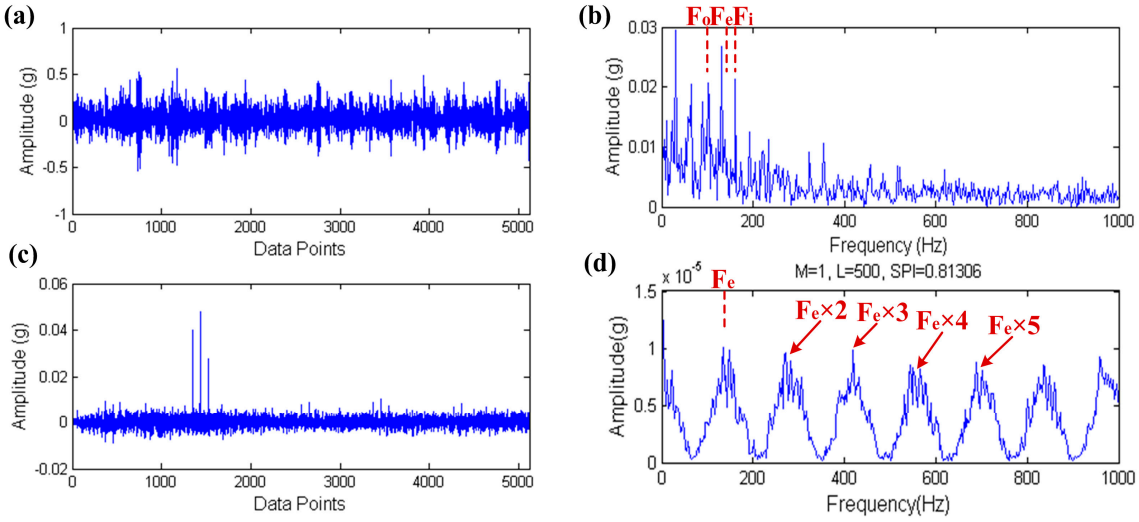

Figure 19. The result of rolling element fault diagnosis: (a) the raw signal; (b) the envelope spectrum of (a); (c) the filtered signal; (d) the envelope spectrum of (c).

6. Conclusions and Future Work

Preprints (www.preprints.org) | NOT PEER-REVIEWED | Posted: 20 January 2017 doi:10.20944/preprints201701.0091.v1

Peer-reviewed version available at Sensors 2017, 17, 535; doi:10.3390/s17030535

This paper mainly introduces a characteristic parameter named SPI, which can be used in fault diagnosis of the REB. Simulation data is used to test the performance of the SPI through these three aspects i.e. the ability of antinoise, resisting the aperiodic impulse and other harmonic components. The performance of the SPI also is compared with kurtosis and Envelope harmonic-to-noise ratio in simulation data. All the results of simulation show that the SPI, as a dimensionless index, has strong ability of diagnosis and it can identify the fault information from the vibration signal effectively, therefore the SPI can yet be regarded as a kind of good characteristic parameter in the application of the REB fault diagnosis. Then, the SPI is applied to the parameter optimization of the MCKD for a set of real vibration data. Through the experimental study of the real vibration signal, the SPI shows a good ability of identification of fault information in the parameter optimization of the MCKD and the result of experimental data indicates clearly the FCF and its high order harmonics, that is to say the SPI as optimization index is feasible. Moreover, the experimental study also shows that the MCKD has a strong ability of deconvolution under the condition of appropriate preset parameters in the REB fault diagnosis and Teager energy operator has a good performance in signal demodulation. On basis of its good performance, Teager energy operator has a brilliant future in the demodulation of the field of mechanical fault diagnosis.

In the future, the SPI, as a good time-domain feature, can be applied to the spectral kurtosis (SK), empirical mode decomposition (EMD), wavelet decomposition (WD) or wavelet packet decomposition (WPD) to identify the fault impulses. What's more, the SPI index is a characteristic parameter, which obtained from a large number of data study. Therefore, the theory of the periodic impulse's physical property also needs to improve and the further work should be focus on the improvement of the theory of periodic impulse' physical property.

Acknowledgments: This work is supported by the National Natural Science Foundation of China (Grant NO. 51575424), and the National Science and Technology Major Project (Grant NO. 2014ZX04001191), which are highly appreciated by the authors. Thanks are also due to the free download of the rolling element bearing fault data sets provided by the bearing data center, Case Western Reserve University.

Author Contributions: Peng Sun and Yuhe Liao conceived and designed the methodology; Peng Sun designed the simulation experiment and analyzed the simulation and real data; Jin Lin provided some valuable advices; Peng Sun and Yuhe Liao wrote the paper.

Conflicts of Interest: The authors declare no conflict of interest.

References

1. Lei, Y. G.;Lin, J.;He, Z. J. and Zuo, M. J. A review on empirical mode decomposition in fault diagnosis of rotating machinery. *Mech. Syst. Signal Process.* **2013**, *35*, 108-126, 10.1016/j.ymssp.2012.09.015.
2. Randall, R. B. and Antoni, J. Rolling element bearing diagnostics—A tutorial. *Mech. Syst. Signal Process.* **2011**, *25*, 485-520, 10.1016/j.ymssp.2010.07.017.
3. Tandon, N. and Choudhury, A. A review of vibration and acoustic measurement methods for the detection of defects in rolling element bearings. *Tribol. Int.* **1999**, *32*, 469-480, 10.1016/s0301-679x(99)00077-8.
4. Miao, Y. H.;Zhao, M.;Lin, J. and Xu, X. Q. Sparse maximum harmonics-to-noise-ratio deconvolution for weak fault signature detection in bearings. *Meas. Sci. Technol.* **2016**, *27*, 105004, 10.1088/0957-0233/27/10/105004.
5. Samanta, B. and Al-Balushi, K. R. Artificial neural network based fault diagnostics of rolling element bearings using time-domain features. *Mech. Syst. Signal Process.* **2003**, *17*, 317-328,

Preprints (www.preprints.org) | NOT PEER-REVIEWED | Posted: 20 January 2017 doi:10.20944/preprints201701.0091.v1

Peer-reviewed version available at Sensors 2017, 17, 535; doi:10.3390/s17030535

10.1006/mssp.2001.1462.

6. Yu, X.;Ding, E. J.;Chen, C. X.;Liu, X. M. and Li, L. A Novel Characteristic Frequency Bands Extraction Method for Automatic Bearing Fault Diagnosis Based on Hilbert Huang Transform. *Sensors* **2015**, *15*, 27869-27893, 10.3390/s151127869.
7. Luo, M.;Li, C. S.;Zhang, X. Y.;Li, R. H. and An, X. L. Compound feature selection and parameter optimization of ELM for fault diagnosis of rolling element bearings. *Isa. T.* **2016**, *65*, 556-566, 10.1016/j.isatra.2016.08.022.
8. Dyer, D. and Stewart, R. M. Detection of rolling element bearing damage by statistical vibration analysis. *Tran. ASME, J. Mech. Des* **1978**, *100*, 229-235, <Go to ISI>://WOS:A1978GF69300004
9. Dwyer, R. F. Detection of non-Gaussian signals by frequency domain Kurtosis estimation. Proceedings of ICASSP 83. IEEE International Conference on Acoustics, Speech and Signal Processing, Boston, MA, USA, 1983;
10. Antoni, J. The spectral kurtosis: a useful tool for characterising non-stationary signals. *Mech. Syst. Signal Process.* **2006**, *20*, 282-307, 10.1016/j.ymssp.2004.09.001.
11. Antoni, J. and Randall, R. B. The spectral kurtosis: application to the vibratory surveillance and diagnostics of rotating machines. *Mech. Syst. Signal Process.* **2006**, *20*, 308-331, 10.1016/j.ymssp.2004.09.002.
12. Antoni, J. Fast computation of the kurtogram for the detection of transient faults. *Mech. Syst. Signal Process.* **2007**, *21*, 108-124, 10.1016/j.ymssp.2005.12.002.
13. Lei, Y. G.;Lin, J.;He, Z. J. and Zi, Y. Y. Application of an improved kurtogram method for fault diagnosis of rolling element bearings. *Mech. Syst. Signal Process.* **2011**, *25*, 1738-1749, 10.1016/j.ymssp.2010.12.011.
14. Barszcz, T. and JabŁoński, A. A novel method for the optimal band selection for vibration signal demodulation and comparison with the Kurtogram. *Mech. Syst. Signal Process.* **2011**, *25*, 431-451, 10.1016/j.ymssp.2010.05.018.
15. Xu, X. Q.;Zhao, M.;Lin, J. and Lei, Y. G. Periodicity-based kurtogram for random impulse resistance. *Meas. Sci. Technol.* **2015**, *26*, 085011, 10.1088/0957-0233/26/8/085011.
16. Xu, X. Q.;Zhao, M.;Lin, J. and Lei, Y. G. Envelope harmonic-to-noise ratio for periodic impulses detection and its application to bearing diagnosis. *Measurement* **2016**, *91*, 385-397, 10.1016/j.measurement.2016.05.073.
17. McDonald, G. L.;Zhao, Q. and Zuo, M. J. Maximum correlated Kurtosis deconvolution and application on gear tooth chip fault detection. *Mech. Syst. Signal Process.* **2012**, *33*, 237-255, 10.1016/j.ymssp.2012.06.010.
18. Jia, F.;Lei, Y. G.;Shan, H. K. and Lin, J. Early Fault Diagnosis of Bearings Using an Improved Spectral Kurtosis by Maximum Correlated Kurtosis Deconvolution. *Sensors* **2015**, *15*, 29363-29377, 10.3390/s151129363.
19. Zhou, H. T.;Chen, J. and Dong, G. M. Engineering Asset Management - Systems, Professional Practices and Certification. Tse, P. W., Mathew, J., Wong, K., Lam, R. and Ko, C. N.; Springer International Publishing: 2015; 159-172.
20. Tang, G. J.;Wang, X. L. and He, Y. L. Diagnosis of compound faults of rolling bearings through adaptive maximum correlated kurtosis deconvolution. *J. Mech. Sci. Tehcnol.* **2016**, *30*, 43-54, 10.1007/s12206-015-1206-7.
21. Liang, M. and Soltani Bozchalooi, I. An energy operator approach to joint application of amplitude

Preprints (www.preprints.org) | NOT PEER-REVIEWED | Posted: 20 January 2017 doi:10.20944/preprints201701.0091.v1

Peer-reviewed version available at Sensors 2017, 17, 535; doi:10.3390/s17030535

and frequency-demodulations for bearing fault detection. *Mech. Syst. Signal Process.* **2010**, *24*, 1473-1494, 10.1016/j.ymssp.2009.12.007.

22. Feng, Z. P.;Liang, M.;Zhang, Y. and Hou, S. M. Fault diagnosis for wind turbine planetary gearboxes via demodulation analysis based on ensemble empirical mode decomposition and energy separation. *Renew. Energy* **2012**, *47*, 112-126, 10.1016/j.renene.2012.04.019.
23. Maragos, P.;Kaiser, J. F. and Quatieri, T. F. On amplitude and frequency demodulation using energy operators. *IEEE. T. Signal. Proces* **1993**, *41*, 1532-1550, 10.1109/78.212729.
24. Maragos, P.;Kaiser, J. F. and Quatieri, T. F. Energy separation in signal modulations with application to speech analysis. *IEEE. T. Signal. Proces* **1993**, *41*, 3024-3051, 10.1109/78.277799.
25. Potamianos, A. and Maragos, P. A comparison of the energy operator and the hilbert transform approach to signal and speech demodulation. *Signal. Process.* **1994**, *37*, 95-120, 10.1016/0165-1684(94)90169-4.
26. Sawalhi, N. and Randall, R. B. Simulating gear and bearing interactions in the presence of faults. *Mech. Syst. Signal Process.* **2008**, *22*, 1924-1951, 10.1016/j.ymssp.2007.12.001.
27. Bearing Vibration Dataset. Available online: http :// csegroups.case.edu / bearingdatacenter / pages / download-data-file (accessed on 8 October 2016).

© 2017 by the authors; licensee *Preprints*, Basel, Switzerland. This article is an open access article distributed under the terms and conditions of the Creative Commons by Attribution (CC-BY) license (http://creativecommons.org/licenses/by/4.0/).